Polymer 51 (2010) 3753–3761

Contents lists available at ScienceDirect

Polymer

journal homepage: www.elsevier.com/locate/polymer

Characterization of melt flow instabilities in polyethylene/carbon nanotube composites

H. Palza [a,*], B. Reznik [b], M. Kappes [c], F. Hennrich [c], I.F.C. Naue [b], M. Wilhelm [b]

[a] Departamento de Ingenieria Quimica y Biotecnologia, Facultad de Ciencias Fisicas y Matematicas, Universidad de Chile, Beauchef 861, Casilla 277, Santiago, Chile
[b] Institut für Technische Chemie und Polymerchemie, Karlsruhe Institute of Technology (KIT), Engesserstrasse 18, 76131 Karlsruhe, Germany
[c] Institut für Nanotechnologie und Institute für Physikalische Chemie, Karlsruhe Institute of Technology (KIT), Hermann von Helmholts Platz 1, 76344, Karlsruhe, Germany

ARTICLE INFO

Article history:
Received 28 April 2010
Received in revised form
27 May 2010
Accepted 7 June 2010
Available online 12 June 2010

Keywords:
Nanocomposites
Melt flow instabilities
Carbon nanotubes

ABSTRACT

The effect of single (SWCNT) and multi- (MWCNT) walled carbon nanotubes on the melt flow instabilities of polyethylenes with different topologies was characterized by means of a novel capillary rheometer allowing in-situ measurements of the pressure fluctuations inside the die and by scanning electron microscopy (SEM) analysis. Our results show that carbon nanotubes modify the main characteristics of the spurt instability developed by the linear polyethylene. Furthermore, the sharkskin instability, developed in short chain branched polyethylene, is reduced at low amounts of MWCNT and SWCNT. Noteworthy, the critical shear rate for the on-set of the spurt and the sharkskin instabilities decreases in the nanocomposites due to the physical interactions between the polymer and the nanofiller.

At high shear rates, the gross melt fracture instability is completely erased in the nanocomposites based on the linear polymer whereas in short chain branched polyethylene the amplitude of this bulk distortion is rather moderated. These changes were confirmed by on-line pressure measurements using the novel capillary rheometer set-up. Based on our results, it is concluded that carbon nanotubes drastically affect the non-linear molecular dynamic leading to polyethylene melt flow instabilities.

1. Introduction

The incorporation of nanoparticles into polymeric matrices is a route to prepare plastic materials with either improved or novel properties [1]. The advantage of adding nanomaterials is often related with the small amount of filler needed to reach the desired behavior. In this context, carbon nanotubes [2] (CNTs) have attracted a large interest due to their extraordinary and unique properties [3,4]. CNTs have one of the highest electrical and thermal conductivities, together with an extremely high tensile modulus and tensile strength [5]. Furthermore, CNTs are characterized by their high flexibility, low mass density, and large aspect-ratio (typically between 300 and 1000) [6,7]. Due to the above mentioned, they are excellent candidates for the fabrication of multifunctional polymeric nanocomposites that could extend the range of application of commodity plastic materials, such as polyethylenes (PE) and polypropylenes (PP).

Examples of the effect of CNTs on the properties (mainly dielectric and mechanical) of polymeric composites can be found elsewhere [8–10]. In general, these properties will depend on several factors e.g., the polymer chemical composition, filler dispersion, aspect-ratio and orientation of CNTs, and interactions between CNTs and the polymer chain [11]. It has been reported that the CNTs increase the glass transition and thermal stability temperatures of the polymer while reducing its overall crystallization [12–22]. Regarding the mechanical properties, tensile tests for polyolefin/CNT composites show important increase in both the Young's modulus and the tensile strength [23–25]. Moreover, the ductility and impact resistance of some CNT composites are larger than the pure polymeric matrix [26–29]. Another property studied in CNT composites is their ability to form a three-dimensional network in polymeric matrices leading to low electrical and rheological percolation thresholds [15,20,29–31].

Despite the extensive range of properties for polymer/CNT composites as above mentioned, there is a lack for a systematic study about their melt flow instabilities. The latter being especially relevant for composites based on commodity matrices as part of these nanomaterials should be melt processed for future commercial applications. Noteworthy, the optimum throughput condition for extrusion processes of polymer/CNT composites will be limited by the appearance of these instabilities [32,33].

There are three main melt flow instabilities depending on the shear rate and the polymer microstructure, namely: sharkskin, spurt (or stick-slip), and gross melt fracture. For a controlled piston

* Corresponding author. Tel.: +56 2 978 40 85; fax: +56 2 699 10 84.
E-mail address: hpalza@ing.uchile.cl (H. Palza).

0032-3861/$ – see front matter © 2010 Elsevier Ltd. All rights reserved.
doi:10.1016/j.polymer.2010.06.016

speed capillary rheometer, at low shear rate the surface of the polymer extrudate is smooth and without any kind of perturbations. Increasing the shear rate, the sharkskin instability could appear consisting of a periodic surface instability with both small amplitudes and high characteristic frequencies [34]. In the flow curve (a plot of the shear rate against the shear stress) this instability is generally associated with a small change in its slope [33,35,36]. At higher shear rates, some polymers present the spurt instability, that it is characterized by periodic smooth/rough regions in the extrudate associated with both a large but slow pressure oscillation inside the barrel and a discontinuity in the flow curve [35,37]. Finally, at high shear rates other instabilities appear which are associated with bulk phenomena and they are called gross melt fracture. The common characteristic of the latter instabilities is its origin in the entrance of the die section due to turbulences or vortex formations in the barrel [33,38,39].

To all our knowledge, only a few articles have reported the effect of CNTs towards these melt flow instabilities [40,41]. In general, it has been shown that the melt flow instabilities are reduced by increasing the amount of CNTs although without a quantitative evaluation about this effect. Moreover, a clear classification of the specific instability studied was missing.

Based on the above mentioned, the aim of this contribution is to study the effect of single- (SWCNT) and multiwalled carbon nanotubes (MWCNT) on the main melt flow instabilities of different polyethylenes. By using a capillary rheometer with a novel detection system for melt flow instabilities and two polyethylenes having different topologies, we are able to characterize spurt, sharkskin, and gross melt fracture flow instabilities in nanocomposites with CNT amount ranging from 0.05 to 12 wt% and from 0.05 to 1 wt%, for MWCNT and SWCNT, respectively. This study is conducted by utilizing our novel set-up for in-situ pressure measurements of melt flow instabilities inside the die with a time resolution Δt of around 1 ms in combination with a pressure resolution ΔP of 1×10^{-4} bar [42–46]. Image analysis from scanning electron microscopy (SEM) characterizing the morphology of the extrudate was further utilized to quantify the morphology of the extrudate.

2. Experimental

To study the whole range of instabilities, two commercial polyethylenes of different topologies were selected. The PE-L sample is a linear high density polyethylene with low amount of long chain branching (3 LCB/1000 CH_2) from Lyondell BASELL and the PE-SCB sample is a ethylene copolymer with 7 mol% of 1-octene (short chain branching) from Dow. The melt flow rates (190 °C/2.16 kg) are: 0.10, and 3.0 g/10 min for PE-L and PE-SCB samples, respectively. The details of topology, molecular weight, melt instability, relaxation time, and melting temperature of the samples are given in Table 1.

The multiwalled carbon nanotubes (MWCNT) were kindly supplied by Bayer Material Science AG (Baytubes C150P). Based on the datasheet information provided by Bayer, they are characterized by a purity higher than 95 wt%, number of walls between 2 and 15, an outer mean diameter of 13–16 nm, an inner mean diameter of 4 nm, length between 1 and >10 μm, and a bulk density around 150 kg/m^3.

Table 1
Main characteristics of the polyethylenes studied.

Sample	Estimated topology	M_w (kg/mol)	M_n (kg/mol)	Melting temperature (°C)	Relaxation time[b] (s)	Main instability
PE-L	Linear	193	20	128.4	0.2	Spurt
PE–SCB	Short chain branching[a]	100	45	99.8	< 0.01	Sharkskin

[a] 6% mol SCB.
[b] Estimated from the cross-over point between the elastic and viscous moluli in a frequency sweep test at 190 °C.

The single walled carbon nanotubes (SWCNT) were prepared by laser vaporization as detailed elsewhere [47]. An Nd:YAG laser irradiated a side surface of a rotating and axially translating composite carbon rod (target) placed in a φ70 mm T-like quartz tube inside a hinge oven. Vaporization was performed at an oven temperature of 1150 °C in 0.5 bar Ar flowing at 80 sccm. SWCNT material was collected on a filter downstream of the oven, in a cold downstream region of the quarts tube along the tubing to the filter.

The dispersion of CNTs in the polymeric matrix was improved by preparing the nanocomposites with a two-steps route. In the first step, the desired amount of CNT was added to a 1,2-dichlorobenzen (DCB, Acros Organic) solution and dispersed gradually during 3 h using a standard VWR ultrasonic cleaner in order to avoid changes in its aspect-ratio. For nanocomposites with content of MWCNT lower than 3 wt%, a CNT concentration of 95 mg/L was used [48]. Other composites were prepared using higher concentrations. Typically, for a composite with 1 wt% of filler, 150 mg of CNT were dissolved in 500 ml of DCB. Additionally, the polymer (15 g) was dissolved in DCB at 120 °C at a concentration of 15 g/L. After the time to dissolve the CNT was elapsed, the CNT solution was heated to 120 °C and added to the polymer solution. The mixture was stirred for 5 min and quickly poured into methanol (Acros Organic) at room temperature and kept it overnight. The precipitate was filtered, dried and putted in an oven with a controlled-temperature (~50 °C) vacuum system to remove the solvent. In the second step, the composites prepared by the solution method were additionally melt-mixed using a HAAKE MiniLab I Micro Compounder from Thermo Scientific with a counter-rotating twin-screw system at 110 RPM. The mixtures were carried out at 210 °C and 140 °C for PE-L and PE-SCB, respectively, for 10 min. By means of this two-steps route, composites with 0.05, 0.1, 0.5, 1.0, 3.0, 6.0, and 12.0 wt% were prepared. Pure PE-L and PE-SCB samples without CNT subjected to this two-steps route condition allowed us to analyze the effect of the processing conditions on their properties (e.g. $G'(\omega)$ and $G''(\omega)$). Significant differences between these pure polymers without any filler and the no-processes pure samples were not detected.

Capillary flow measurements were carried out in a GÖTTFERT Rheo-tester 2000 capillary rheometer at 190 °C and 140 °C for composites based on PE-L and PE-SCB, respectively. Both the shear stress and the shear rate were measured without any correction (e.g. Bagley or Rabinowitch). The slit-die used in this work is home-made and non-conventional (see Fig. 1) although now it is also commercially available via Göttfert. It was specifically designed in order to allow the evaluation of fast and minor pressure fluctuations at three different locations along its length, at 3, 15 and 27 mm and named T1, T2 and T3 respectively. Details about this new and unique set-up and the mathematical framework to process its pressure data are reported elsewhere [42–45]. The limit time resolution Δt is typically 1 ms and 1×10^{-4} bar for pressure resolution ΔP. Fourier analysis is performed on the time dependent pressure data, and the observed peaks at the frequency-domain are located at frequencies that are the inverse of the related time scale of the instability. All the experiments were repeated at least twice to ensure reliability of the tendencies found through the article.

The viscoelastic properties of the samples were obtained in an ARES rheometer from TA Instruments using parallel plate configuration with a diameter of 25 mm at temperatures of 140° and 190 °C, for PE-L and PE-SCB, respectively. Oscillatory shear experiments in the linear regime were conducted in a frequency range from 10^{-2} to 10^2 rad s^{-1}, under nitrogen atmosphere.

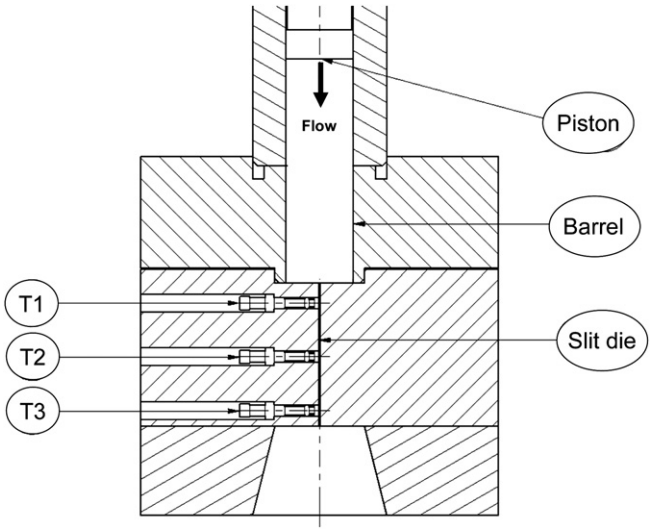

Fig. 1. Technical drawing of the home-made slit-die designed with three high sensitive pressure transducer inside the slit (0.3 × 3 × 0.3 mm^3), labeled as T1, T2 and T3.

The morphology of the polymer/carbon nanotube composites was investigated using a Hitachi S-570 scanning electron microscope (SEM) operated with an accelerating voltage of 25 kV. SEM observations were made from samples whose surface was vacuum-metallized with a Au conductive layer. The "Image J" software package was used for the quantitative analysis of SEM micrographs [49]. The specific density of cell boundaries is the parameter evaluated from the pictures. It is calculated by correlating the total length of the cell boundaries relative to the total area studied. A cell network is defined by the boundaries of the distortions appearing in the extrudate. In our case, these boundaries represent both a closed cell and an open structure. From reconstructed binary micrographs a total value of black pixels (representing the cell boundaries) is related to the measured total area of the micrograph.

3. Results and discussions

3.1. Melt viscoelasticity

Figs. 2 and 3 show the elastic (G′) and the viscous moduli (G″) of the composites based on PE-L and PE-SCB with MWCNT, respectively. Increasing the amount of MWCNT a slight increase in the moduli is observed in PE-L composites. There is no evidence about a solid-like transition even in the sample with 12 wt% of MWCNT. A clear difference is observed in composites based on PE-SCB as a rheological percolation appears at filler concentrations higher than 1 wt%. The PE-SCB sample with the highest amount of filler displays at low frequencies (~0.1 rad/s) elastic (G′) and viscous (G″) moduli that are four and two orders of magnitude larger than the neat sample, respectively. Moreover, this composite displays a frequency-independent moduli and the elastic response becomes larger than the viscous response reflecting the transition from a liquid-like to a solid-like behavior.

The dispersion degree of CNT in the polymer matrix strongly affects the viscoelastic response of the composite at melt state [50]. Therefore, the behavior observed in PE-L composites could be explained by a poor dispersion of CNT in the composites. Nevertheless, the melt dynamic properties (e.g. the longest relaxation time as displayed in Table 1) and the molecular weight of the matrix should be further considered. It is well known that the effect of the nanofiller is dominantly observed at low frequencies where the polymer is able to relax and the short-range physical interactions between the MWCNT and the polymer become important [11]. Due to the presence of small amounts of long chain branching in PE-L, the terminal zone (characterized by $G' \propto \omega^2$ and $G'' \propto \omega^1$) is not yet observed in Fig. 2 and the polymer does not fully relax within the tested time scale [51]. Therefore, it is not possible to observe the solid-like transition in this sample in our frequency range. The opposite is found in PE-SCB and its terminal zone is observed in Fig. 4. This approach is supported by the electrical conductivity behavior (not shown in this contribution) of the nanocomposites based on PE-L. An electrical percolation transition at concentrations ~6 wt% is observed in these composites meaning that CNT are well disperse and are able to form a 3-D interconnected network through the matrix. On the other hand, the molecular weight (see Table 1) is another factor changing the behavior of these nanocomposites as the load transfer between the polymer and the CNT and the rheological constrains of the polymer chains are affected by this parameter [11,52]. PE-L presents a higher molecular weight than PE-SCB, therefore it needs more filler to display similar behavior than PE-SCB [52].

Despite the above mentioned regarding differences in filler dispersion, viscoelastic behavior, and chain molecular weights, the CNT are able to interact with the polymer chains modifying drastically the melt flow instabilities of both matrices as our findings show (see below for details).

3.2. Spurt instability

The flow curves for PE-L and its composites with high amounts of MWCNT are displayed in Fig. 4. The data for the other samples are

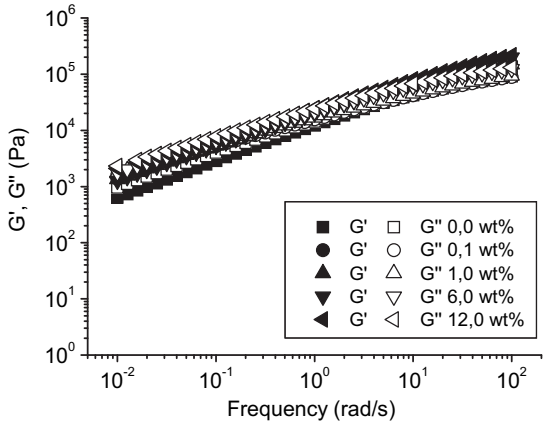

Fig. 2. Elastic (G′) and viscous (G″) moduli for PE-L and some of its composites with MWCNT measured at 190 °C.

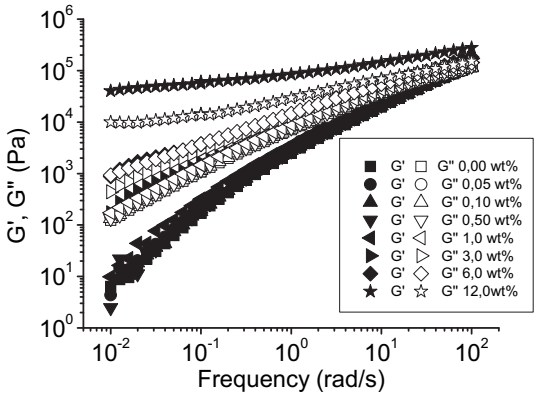

Fig. 3. Elastic (G′) and viscous (G″) moduli for PE-SCB and its composites with MWCNT measured at 140 °C.

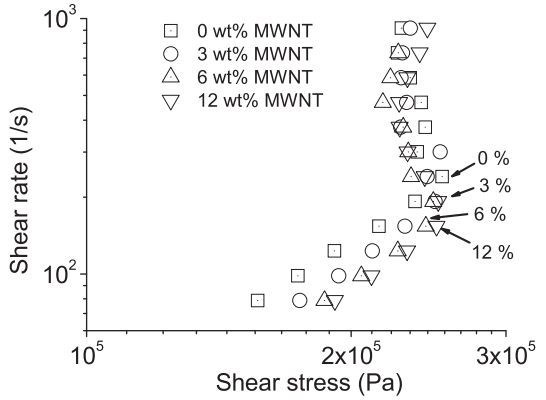

Fig. 4. Flow curve for PE-L and its composites with high amount of MWCNTs measured at 190 °C. The arrows indicate the on-set of the spurt instability.

not shown as they display the same tendency. The pure PE-L develops the spurt instability at shear rates higher than 250 s^{-1} as a discontinuity in the flow curve is observed around this point [44]. Moreover, large but slow pressure fluctuations of approximately 10% with respect to the mean value are detected even by the conventional transducer located inside the barrel at shear rates higher than 250 s^{-1}. These large but slow fluctuations are related with the appearance of alternated smooth/rough regions in the extrudate as it is well known for the spurt instability [44,53–55]. From Fig. 4, it is also observed that increasing the amount of MWCNT in the PE-L matrix, the shear rate for the on-set of the instability decreases. The last finding is better observed by plotting the critical shear rate ($\dot{\gamma}_c$) and shear stress (σ_c) for the on-set of the spurt instability against the filler content for all samples (Fig. 5). By increasing the amount of MWCNT, $\dot{\gamma}_c$ decreases proportionally to its content. This critical shear rate can be reduced about 40% respects to the original value in samples with the highest amount of filler. The shear stress threshold for the on-set of the spurt instability nevertheless keeps constant, independent of the MWCNT content.

It is possible to understand the spurt instability as a reversible transition from a stick to a slip condition in the fluid at the die-wall. Based on the model of Brochard and de Gennes [56], this transition can be related with changes in the forces acting on adsorbed or grafted chains at a wall due to the surrounded polymers. To discuss our findings, one tethered chain in a flowing melt at the low grafting density limit is considered [56]. This simple analysis gives the basic principles to quantitatively understand our phenomena. In this case, the total friction force acting on a grafted chain is [57]:

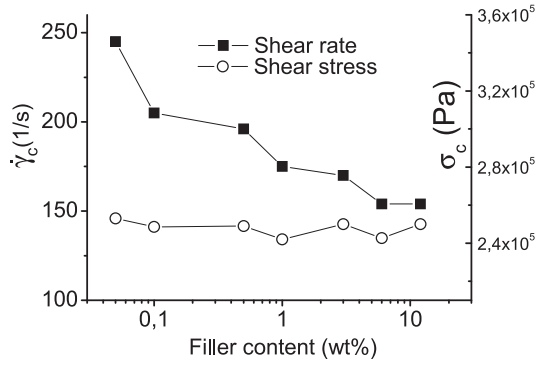

Fig. 5. Effect of the MWCNT content on the critical shear rate ($\dot{\gamma}_c$) and shear stress (σ_c) for the on-set of the spurt instability in PE-L samples at 190 °C.

$$F_v = X \cdot a \cdot \eta_p \cdot V \tag{1}$$

where X is the number of mobile chains from the melt trapped with the tethered chain; V is the velocity of the mobile chains with respect to the grafted chain; a is the molecular size of the monomer with length units; and η_p is the viscosity of the melt. At high velocities is possible to show that the grafted chain will have a cigar-shape with a mean diameter D of [57]:

$$D = \frac{\tilde{k} \cdot T}{F_v} \tag{2}$$

where $\tilde{k}$ is a constant and T is the absolute temperature. From the above mentioned, it is concluded that increasing the velocity of the fluid the diameter of the tethered molecule decreases. At a threshold velocity, V^*, the named marginal regime is reached where the diameter of the grafted polymer is the minimum, D^*, necessary to entangle with the melt [56,57]:

$$D(V^*) = D^* \propto a \cdot N_e^{1/2} \tag{3}$$

where N_e is the number of monomers per entanglement. At velocities higher than V^*, the polymer will disentangle from the surround molecules (slip process), therefore the drag force on the chain will decrease, increasing D and allowing the entanglements again (stick process). In this way, a reversible process occurs at these velocities called coil–stretch transition. From the last equation, it is possible to gain the following expression:

$$V^* = \frac{k \cdot T}{X \cdot N_e^{1/2} \cdot a^2 \cdot \eta_p} \tag{4}$$

where k is a constant. To simplify our analysis, we state that by reaching the so called marginal regime, the fluid suffers the transition from the stick to the slip condition at the wall meaning macroscopically the spurt instability.

Due to the interactions between the MWCNT and the polymer [11,58], we can assume that in the nanocomposite the total frictional force on the tethered polymer is now:

$$F_v = X \cdot a \cdot \eta_p \cdot V + X_{CNT} \cdot k_{CNT} \cdot V \tag{5}$$

where X_{CNT} is the number of MWCNT interacting with the tethered chain and k_{CNT} is a constant. A simple linear relationship between the frictional forces on the polymer due to MWCNT and the filler velocity is therefore postulated. It is also assumed that the velocity of the fluid is the same as the velocity of the MWCNT. Based on the above mentioned, the new velocity V^*_{CNT} necessary to reach D^* in the nanocomposites is:

$$V^*_{CNT} = \frac{k \cdot T}{N_e^{1/2} \cdot a \cdot \left(X \cdot a \cdot \eta_p + X_{CNT} \cdot k_{CNT}\right)} < V^* \tag{6}$$

Therefore, due to the interactions between the MWCNT and the polymers adsorbed at the wall, the velocity necessary to reach the marginal regime is lower and inversely proportional to the concentration of filler, confirming our results (Figs. 4 and 5). Furthermore, the critical force needed to reach the marginal regime should not be changed in the nanocomposites, explaining the behavior observed in Fig. 5 for the critical shear stress. By adding other relationships for the new forces on the grafted polymer due to the MWCNT, the main conclusion of this analysis is not altered.

There is a different approach to understand Fig. 5 based on a kinetic argumentation. It has been reported that a second condition for the stick-slip process is that the tube evacuation time of a bulked-chain to disentangle from the grafted chain (T_{rep}) should be lower than the relaxation time of the bulk polymers

(τ_{bulk}) [57]. As the presence of MWCNT increases the viscosity of the melt that surround the grafted chains, rising τ_{bulk}, the critical velocity of the fluid allowing to T_{rep} be lower than τ_{bulk} will decrease with the content of CNTs because $T_{rep} \propto 1/V$ [57].

The presence of MWCNT in the polymer also modifies the relative pressure fluctuation associated with the stick/slip cycles measured as the ratio between the standard deviation of the pressure oscillation and its mean value [44,59]. By increasing the amount of MWCNT, the relative pressure fluctuation at a shear rate of 315 s^{-1} increases reaching a plateau approximately of 5.5% at concentrations higher than 1 wt% as displayed in Fig. 6. This effect is due to the larger total frictional force on the chains when the amount of MWCNT increases meaning that at a same shear rate the nanocomposites will have a larger shear stress field than the neat polymer. It has been shown recently [44] that by increasing the shear rate (or the shear stress) in pure PE-L, the relative pressure fluctuation of the stick/slip transition is increased in agreement with our results for the nanocomposites. Therefore, the nanocomposites at 315 s^{-1} behave as the pure matrix at a higher shear rate.

A summary of the effect of the MWCNT on the spurt instability behavior is displayed in Table 2.

3.3. Sharkskin instability

PE-SCB develops sharkskin instability as a surface distortion was observed in the extrudate at low shear rates. As it has been proposed, the on-set of this instability can be related with a change in the slope of the flow curve [33,35,36]. Based on this change, it is found that the presence of MWCNT decreases the shear rate for the on-set of the sharkskin instability as displayed in Fig. 7, similar to the effect on the spurt instability. Moreover, the shear stress is again unrelated with the filler content. Therefore, both instabilities can be triggered by a critical shear stress that is reached at lower shear rates due to the presence of MWCNT increasing the total frictional force on the chains (see equation (5)). It is highlighted that even if composites based on PE-L and PE-SCB display differences in the filler dispersion still both matrices should present physical interactions with CNT although quantitatively different.

Several theories explaining sharkskin instability have been reported. Some theories are based on the singularity in the flow dynamic of the polymer around the die-exit due a high velocity gradient as the flow evolves from a shear flow with no-slip boundary condition to a plug flow with free surface boundary condition. This singularity could produce a fast melt rupture in the polymer at the die-exit [34] or a coil–stretch transition in a zone still inside the die but very close to its exit [35]. Other theories explaining sharkskin instability are based on the constitutive origin of the sharkskin instability inside the die as some experimental results seem to support [53,60,61]. Despite the lack of a unified mechanism explaining sharkskin instability, all the above mentioned theories explicitly define a critical force for the on-set of the distortion that is reached at lower shear rates when the MWCNT are added.

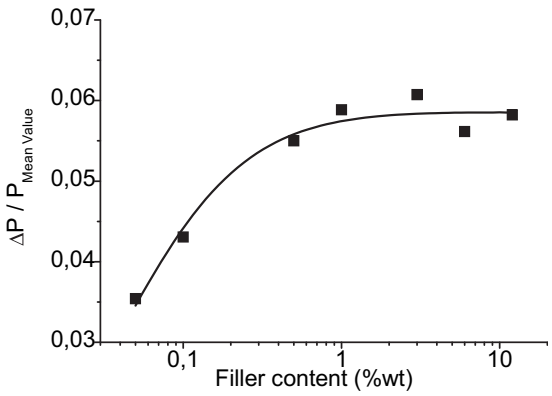

Fig. 6. Effect of the MWCNT content on the relative pressure fluctuation of the spurt instability of PE-L samples at a shear rate of 315 s^{-1} ΔP and $P_{Mean\ value}$ are the standard deviation and the mean value of the pressure signal, respectively.

To evaluate the effect of the MWCNT on the behavior of the sharkskin instability, SEM images of the composites processes at a shear rate of 472 s^{-1} were taken. Some representative images are displayed in Fig. 8. Important changes in the morphology of the extrudate are observed depending on the amount of MWCNT. At low filler content, the composites present reduced surface instability amplitudes (Fig. 8b) compared with the neat sample (Fig. 8a). Increasing the filler content, in particular at concentrations of MWCNT higher than 3 wt%, an opposite effect is observed as the surface instability presents distortions similar to the neat polymer that it can become even slightly stronger in the case of the composite with the highest amount of filler (Fig. 8c and d). The larger forces acting on the polymer by the presence of the MWCNT (see equation (5)) can trigger phenomena occurring in the neat polymer at higher shear rates. The latter meaning that the nanocomposites with high MWCNT content can develop a sharkskin with characteristics related with higher shear rates or some kind of gross melt fracture, similar to the found in PE-L under spurt instability. This is supported by recently results showing that the main characteristics of the melt instabilities are shear rate dependent in these samples [44].

The specific density of cell boundary was measured from SEM images for each sample processed at 472 s^{-1} quantifying the changes in the polymer morphology. A summary of these results is displayed in Fig. 9. From this figure is clear that composites with a filler amount lower than 1 wt% present a specific density of cell boundaries that are below the value corresponding to the neat sample meaning a reduced distortion in the micrograph. The lowest distortion occurs at a filler concentration of 0.1 wt%. At higher concentrations the samples display values that are close to the neat sample. This figure supports the effect of MWCNT on the sharkskin morphology, showing that the low amount of filler is able to reduce the surface distortion. Another parameter that was evaluated from SEM images is the characteristic length of the instability. For this purpose, Fourier analysis was carried out to the SEM images

Table 2
Summary of the effect of CNT on the main melt flow instabilities of polyethylenes.

Polyethylene topology	Concentration of CNT	Spurt	Sharkskin	Gross melt fracture
Linear	Low	Not affected	N/A	Not affected
	High	Larger pressure fluctuations and lower $\dot{\gamma}_c$	N/A	Erased
Short chain branched	Low	N/A	Reduced surface distortion	Not affected
	High	N/A	Larger surface distortion and characteristic length, and lower $\dot{\gamma}_c$	Reduced distortion

$\dot{\gamma}_c$: Critical shear rate for the on-set of the instability; the limit between low and high concentrations of CNT is ~1 wt%. For details see the text.

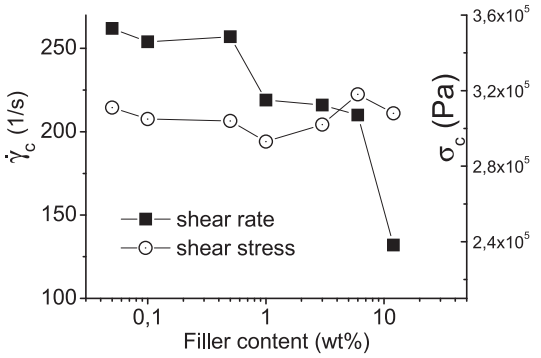

Fig. 7. Effect of the MWCNT content on the critical shear rate ($\dot{\gamma}_c$) and shear stress (σ_c) for the on-set of the sharkskin instability in PE-SCB/MWCNTs composites at 140 °C.

allowing the quantification of the number of instabilities per image [62]. The inverse of the main peak displayed in the Fourier space gives the characteristic length of the instability, as displayed in Fig. 10. From the latter figure is clear that with MWCNT the characteristic length of the instability increases until a ~50%. Furthermore, the lowest characteristic length is for the composite with 0.1 wt%, in agreement with the results from the specific density of cell boundaries.

To evaluate the effect of the structure of carbon nanotube on this instability, composites of PE-SCB with SWCNT having concentrations ranging from 0.05 to 1.0 wt% were prepared. Although at these concentrations of filler it was not possible to detect any change in the critical shear rate for the on-set of the instability, the presence of SWCNT is able to reduce the surface instability at low concentrations as observed in Fig. 8e. Therefore, carbon nanotubes can reduce the sharkskin distortion at low concentrations independent of its characteristics. Furthermore, at 1 wt% of SWCNT the surface instability is stronger than the neat sample (Fig. 8f), similar to the observed at higher concentrations of MWCNT. A summary of the effect of the MWCNT on the spurt instability behavior is displayed in Table 2.

3.4. Gross melt fracture

At high shear rates the samples develop gross melt fracture that it is characterized by a bulk distortion in the extrudate [44]. Using the novel set-up based on three transducers located inside the die and applying advanced mathematical tools to process the time

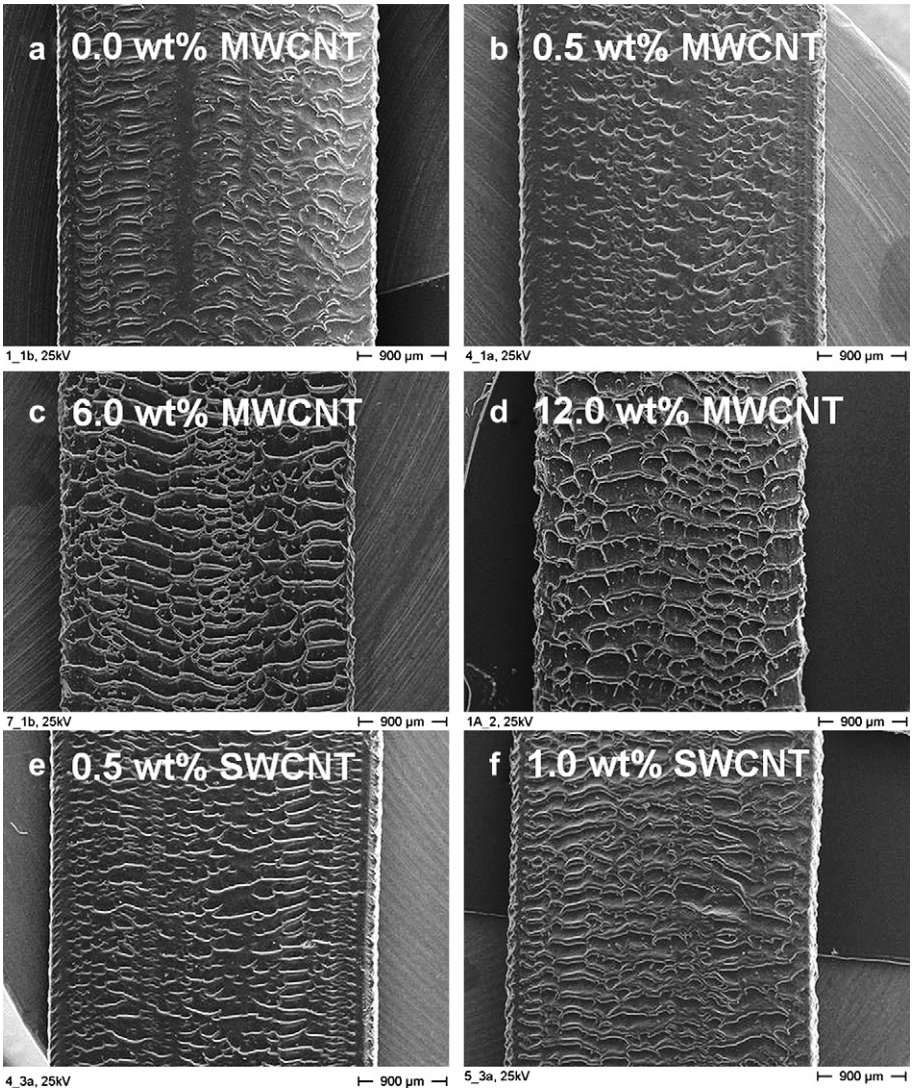

Fig. 8. SEM images showing the effect of carbon nanotube on the surface morphology of PE-SCB composites processed at a shear rate of 472 s^{-1}. Under these conditions the samples develop sharkskin instability.

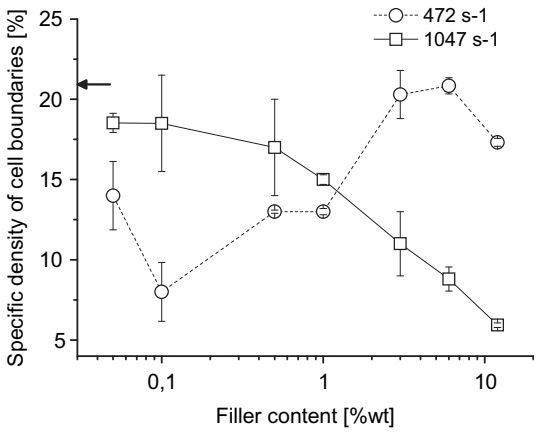

Fig. 9. Effect of MWCNT and shear rate on the specific density of cell boundaries for PE-SCB composites: a) circles correspond to a shear rate of 472 s^{-1} and b) square corresponds to a shear rate of 1047 s^{-1}. The arrow indicates the value of the pure polymer at 472 s^{-1}.

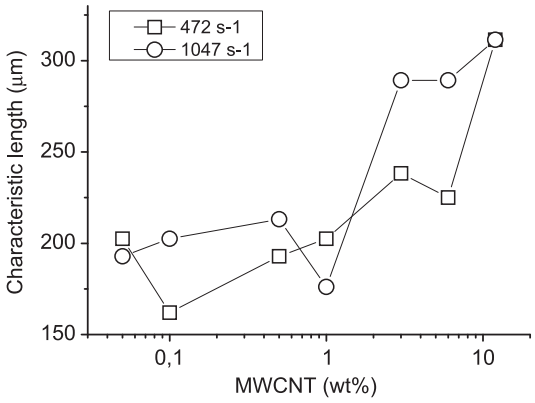

Fig. 10. Effect of the MWCNT on the characteristic length of the instability as measured from Fourier analysis of the SEM images.

dependent pressure signal, it is possible to detect in-situ the pressure fluctuations coming from this instability [42–44,53].

Regarding the composites based on the linear PE-L, Fig. 11 shows representative Fourier transforms of the pressure fluctuation ($P(t)$) measured inside the die at a shear rate of 2047 s^{-1} [42,44,46,53,63]. Under this condition, the pure PE-L develops gross melt fracture and the peak appearing in Fig. 11a at a frequency of 30 Hz is related with the period of this instability in the extrudate [44]. Composites with low amount of filler not only show the same main peak at 30 Hz but also one of its harmonics at 60 Hz (Fig. 11b) [44]. Noteworthy, composites with filler content higher than 1 wt% do not show any peak in the Fourier transform of their pressure signals, as it is observed in Fig. 11c and d. The absence of a characteristic peak in the Fourier spectra means that the pressure fluctuation associated with the instability is either drastically diminished or changed to a higher characteristic frequency out of the range of our set-up. Nevertheless, the extrudates associated with these composites are smooth and evidences of irregularities coming from melt instabilities could not be observed. Therefore, the gross melt fracture is not developed in composites with MWCNT content higher than 1 wt% at a shear rate of 2047 s^{-1} as additionally detected by the suppression of the pressure fluctuations inside the die. It has been recently shown a similar tendency in polyethylene/clay nanocomposites [64], where the gross melt fracture is delayed to higher shear rates due to the higher elastic properties of the composites resisting large elongational stresses. Noteworthy, this result means that nanocomposites based on high density polyethylenes and carbon nanotubes can have larger throughout in extrusion processes with highly economical and environmental consequences.

The effect of MWCNT on the gross melt fracture of PE-L has another relevant consequence related with the lack of any effect of the filler in the linear viscoelastic measurements displayed in Fig. 2. Furthermore, composites based on PE-L display an electrical percolation at filler concentration higher than 6 wt%, as it will be reported in a next contribution. Therefore, similar to other molecular characteristics of the polyethylenes such as small amount of long chain branching in polyethylene [65], mechanical linear

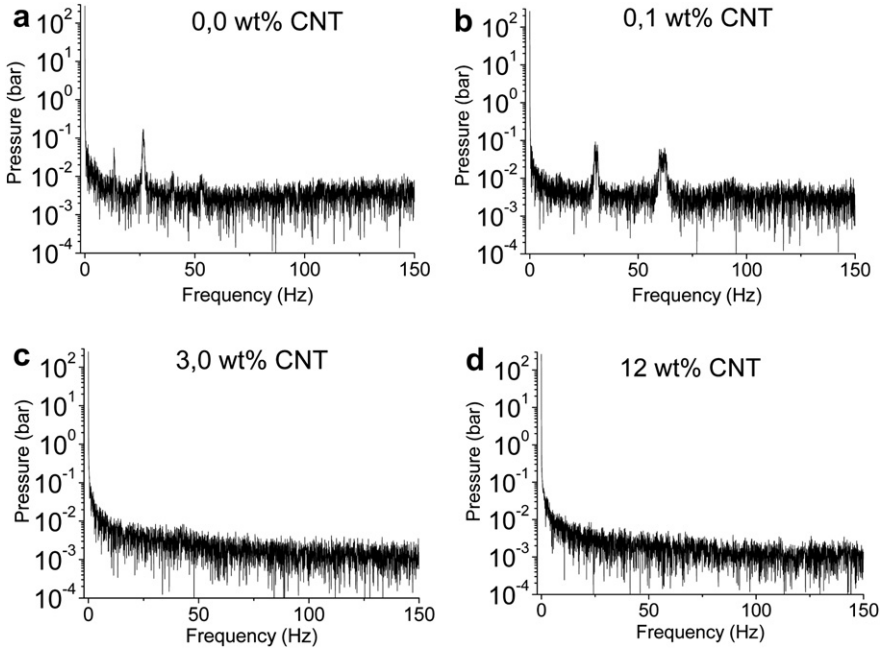

Fig. 11. Fourier transform of the pressure fluctuation associated with gross melt fracture instability for composites based on PE-L at a shear rate of 2047 s^{-1}.

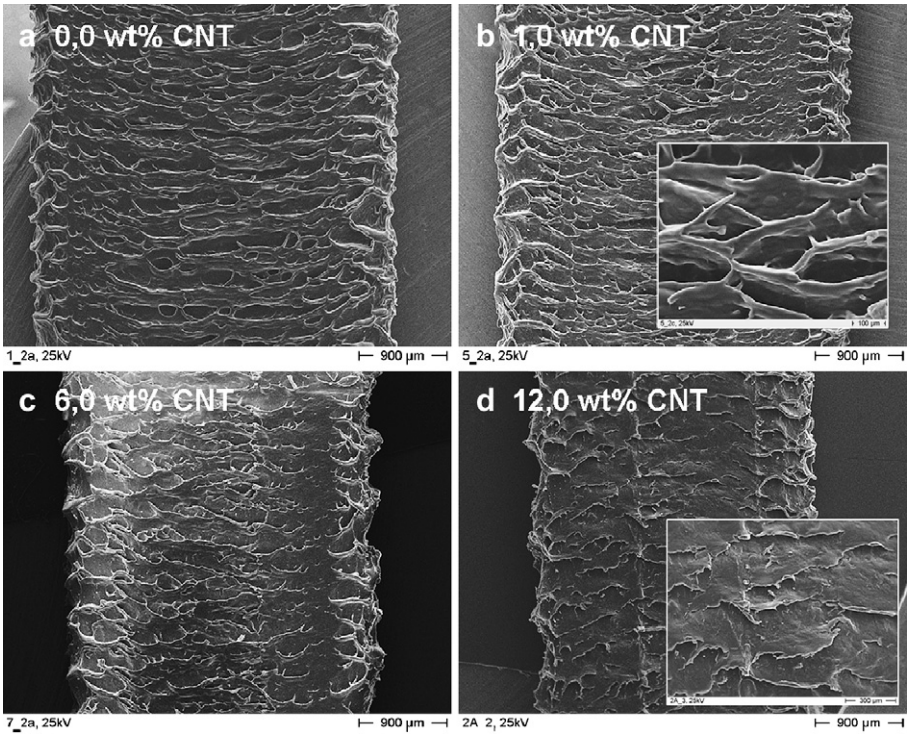

Fig. 12. SEM images showing the effect of MWCNTs amount on the surface morphology of PE-SCB composites processed at a shear rate of 1054 s^{-1}. Under these conditions the samples develop gross melt fracture. Insets in (b) and (d) demonstrate detailed morphological changes occurring with increasing MWCNTs amount.

measurements of G′ and G″ are not enough to fully characterize the filled polyethylenes.

Analyzing the SEM images of the composites based on PE-SCB processed at a shear rate of 1047 s^{-1}, the effect of CNTs on the gross melt fracture for short chain branched samples is further studied (Fig. 12). The neat polymer shows the characteristic morphology of this instability with strong bulk distortions as opposed to the surface instability observed at 472 s^{-1}. The characteristic frequency measured by the Fourier transform of the associated pressure signal is localized at 61 Hz. Composites with low amount of filler do not show any difference in the morphology compared with the neat polymer as it is concluded from Fig. 12a and b. Moreover, these composites presented pressure fluctuations inside the die with the same characteristic frequency and mean value as the neat polymer. At concentrations of MWCNT higher than 3 wt%, drastic changes in the morphology are observed (e.g. Fig. 12c and d). The effect on the morphology of MWCNT is confirmed analyzing the specific density of cell boundaries displayed in Fig. 9 for all the nanocomposites where a systematic decreases, proportional to the filler content, is clearly observed. Furthermore, the characteristic length shows an increase with the MWCNT, similar to the observed for sharkskin (Fig. 10).

In composites based on PE-SCB with concentrations of MWCNT higher than 3 wt%, the Fourier transform of the pressure signal is not able to detect any characteristic peak in our frequency range. Therefore, similar to the observed in PE-L based composites with high filler content, exist a threshold concentration of filler suppressing the dynamic of the pressure fluctuation inside the die. But despite the absent of a signal detection of these pressure fluctuations, the composites based on the PE-SCB display surface distortions even at the highest content of MWCNT. The last could be due to an important reduction of the pressure fluctuation inside the die to levels lower than the sensitivity of our novel set-up, but that it could allow anyway the appearance of distortions in the extrudate. A summary of the effect of the MWCNT on the spurt instability behavior is displayed in Table 2.

From Fig. 12 is not only possible to observe the drastic change in the morphology between the samples but also the suppression in the die-swell phenomenon [41]. It has been reported that the MWCNT are able to produce a negative first normal stress difference in the polymers. This change in the normal stress generates a contraction of the fluid exiting the die by a suppression of the die-swell [41]. In our case, the extrudate contraction relative to the pure polymer is evident at polymers with high MWCNT content (Figs. 8d and 12d). To evaluate indirectly the change in the first normal stresses, the relative ratio (RR) defined as the ratio between the width of the composite and the width of the slit was measured for all the samples at the different shear rates. The PE-L sample processed at 2047 s^{-1} continuously decrease its RR while increasing the amount of filler from 1.5 to 1.3, for the neat polymer and the composite with 12 wt% of MWCNT, respectively. The PE-SCB sample displays a similar behavior as MWCNT are able to reduce its RR from 1.06 to 0.91 for the neat sample and the composite with the highest amount of filler, respectively, when is processed at 432 s^{-1}. At 1047 s^{-1} these changes are larger: from 1.2 to 0.92. The strong reduction in the composite width with the content of MWCNT confirms that the incorporation of the nanofiller decrease the die-swell effect. This reduction in the die-swell can further explain some morphology changes in the melt instabilities above discussed such as gross melt fracture instability in PE-SCB at 1047 s^{-1}.

4. Conclusions

The effect of the addition of carbon nanotubes on the polymer melt flow instabilities was studied by a specially modified GÖTTFERT capillary rheometer and a scanning electron microscopy (SEM) coupled with digital image analysis. Composites based on the linear polyethylene present spurt instability and the addition of

MWCNT decreases the critical shear rate for the on-set of this instability although the shear stress threshold is not altered. The last findings are explained by the interactions between the filler and the polymer increasing the frictional forces. The amplitude of the pressure fluctuations associated with stick/slip processes are raised with the addition of the filler.

Samples based on the polyethylene with short chain branching develop the sharkskin instability. Similar to the spurt instability, the increase of MWCNT reduces the critical shear rate for the on-set of this instability, as higher forces are present on the polymer due to the nanofiller. At filler concentrations lower than 1 wt%, the sharkskin distortion is reduced but at higher contents a more drastic distortion is developed and the characteristic length of the instability is increased as observed by SEM. This tendency is a general behavior of carbon nanotubes as SWCNT display the same effect. Therefore, low amount of single- and multiwalled carbon nanotubes are able to reduce the sharkskin instability at low concentrations.

Independent of the polymer microstructure, the addition of MWCNT drastically modifies the gross melt fracture instability found at high shear rates. In composites based on linear PE-L this instability is completely erased at high amounts of filler and evidences of this distortion in the extrudate is not found. Therefore MWCNT can increase the throughput of extrusion processes. In composites based on the short chain branched PE-SCB, the amplitude of the distortion associated with this bulk instability is drastically reduced. These results are supported by in-site pressure measurements inside the slit-die showing that at concentrations of MWCNT higher than ~3 wt%, the pressure fluctuations associated with gross melt fracture are note detected.

By measuring the values of the specific density of cell boundaries extracted from reconstructed SEM micrographs, the quantification of the above mentioned surface distortions as function of filler content was possible for PE-SCB composites. This parameter confirms the strong effect of MWCNT on the distortions from the extrudate.

By means of our findings a clear effect of the carbon nanotubes on the main melt flow instabilities observed in polyethylenes is concluded. This effect depends of the specific instability that it is analyzed and of the concentration of filler, as summarized in Table 2.

Acknowledgements

The authors gratefully acknowledge the financial support of CONICYT, project FONDECYT INICIACION EN INVESTIGACION 11075001, the support of the Alexander von Humboldt Foundation as well as the support of the DFG-Priority program 1299: “Adapting surfaces for high temperature applications”. An acknowledgment is due to Thermo Scientific for providing us with the mini extruder and to Bayer Material Science AG, specifically to Dr. H. Meyer, for providing the CNTs. We would like to thanks the GOTTFERT GmbH, specifically to Dr. J. Sunder and DR. A. Gottfert, for making our ideas toward this special set-up commercially available. The authors are also grateful to Prof. H. Bockhorn for the provision of laboratory facilities for SEM investigations.

References

[1] Paul DR, Robeson LM. Polymer 2008;49:3187–204.
[2] Iijima S. Nature 1991;354:56–8.
[3] Terrones M. Int Mat Rev 2004;49:325–77.
[4] Krupke R, Hennrich F, von Lohneysen H, Kappes MM. Science 2003;301:344–7.
[5] Ajayan PM. Chem Rev 1999;99:1787–99.
[6] Moniruzzaman M, Winey KI. Macromolecules 2006;39:5194–205.
[7] Pötschke P, Dudkin SM, Alig I. Polymer 2003;44:5023–30.
[8] Coleman JN, Khan U, Gun'ko YK. Adv Mater 2006;18:689–706.
[9] Thostenson ET, Ren Z, Chou TW. Comp Sci Tech 2001;61:1899–912.
[10] Lau K, Gu C, Hui D. Composites Part B 2006;37:425–36.
[11] Du F, Scogna RC, Zhou W, Brand S, Fisher JE, Winey KI. Macromolecules 2004;37:9048–55.
[12] Gong X, Liu J, Baskaran S, Voise RD, Young J. Chem Mater 2000;12:1049–52.
[13] Bao SP, Tjong SC. Mater Sci Eng A 2008;485:508–16.
[14] Valentini L, Biagiotti J, Kenny JM, Santucci S. Compos Scien Tech 2003;63:1149–53.
[15] Seo MK, Lee JR, Park SJ. Mater Sci Eng A 2005;404:79–84.
[16] Bhattacharyya AR, Sreekumar TV, Liu T, Kumar S, Ericson LM, Hauge RH, et al. Polymer 2003;44:2373–7.
[17] Lee GW, Jagannathan S, Chae SH, Minus ML, Kumar S. Polymer 2008;49:1831–40.
[18] Assouline E, Lustiger A, Barber AH, Cooper CA, Klein E, Watchtel E, et al. J Polym Sci Part B Polym Phys 2003;41:520–7.
[19] Kodjie SL, Li L, Li B, Cai W, Li CY, KeatingMacromol MJ. Scie Part B Phys 2006;45:231–45.
[20] Jeon K, Lumata L, Tokumoto T, Steven E, Brooks J, Alamo R. Polymer 2007;48:4751–64.
[21] Kashiwagi T, Grulke E, Hilding J, Harris R, Awad W, Douglas J. Macroml Rapid Commun 2002;23:761–5.
[22] Kashiwagi T, Grulke E, Hilding J, Groth K, Harris R, Butler K, et al. Polymer 2004;45:4227–39.
[23] Lopez-Manchado MA, Valentini L, Biagiotti J, Kenny JM. Carbon 2005;43:1499–505.
[24] Xiao KQ, Zhang LC, Zarudi I. Comp Scie Techn 2007;67:177–82.
[25] Chang TE, Jensen LR, Kisliu A, Pipes RB, Pyrz R, Sokolov AP. Polymer 2005;46:439–44.
[26] Zang H, Zang Z. Europ Polym J 2007;43:3197–207.
[27] Kanagaraj S, Varanda FR, Zhiltsova TV, Oliveira MSA, Simoes JAO. Composites Scie Techn 2007;67:3071–7.
[28] Zhao P, Wang K, Yang H, Zhang Q, Du R, Fu Q. Polymer 2007;48:5688–95.
[29] McNally T, Potschke P, Halley P, Murphy M, Martin D, Bell SEJ, et al. Polymer 2005;46:8222–32.
[30] Nobile MR, Simon GP, Valentino O, Morcon M. Macromol Symp 2007;247:78–87.
[31] Zhang Q, Rastogi S, Chen D, Lippits D, Lemstra PJ. Carbon 2006;44:778–85.
[32] Larson RG. Rheol Acta 1992;31:213–63.
[33] Denn MM. Ann Rev Fluid Mech 2001;33:265–87.
[34] El Kissi N, Piau JM. J Rheology 1994;38:1447–63.
[35] Wang SQ. Adv Polym Sci 1999;138:227–75.
[36] Hill DA, Hasegawa T, Denn MM. J Rheology 1990;34:891–918.
[37] Wang SQ, Drda P. Macromolecules 1996;29:2627–32.
[38] Legrand F, Piau JM. J Non-Newtonian Fluid Mech 1998;77:123–50.
[39] Tao Z, Huang JC. J Appl Polym Sci 2005;98:903–11.
[40] Xu DH, Wang ZG, Douglas J. Macromolecules 2009;41:815–25.
[41] Kharchenko SB, Douglas JF, Obrzut J, Grulke EA, Migler KB. Nat Mat 2004;3:564–8.
[42] Filipe S, Vitorias I, Wilhelm M. Macromol Mat Eng 2008;293:57–65.
[43] Filipe S, Becker A, Barroso V, Wilhelm M. App Rheol 2009;19:23345.
[44] Palza H, Filipe S, Naue IFC, Wilhelm M. Polymer 2010;51:522–34.
[45] Palza H, Naue IFC, Filipe S, Becker A, Sunder J, Göttfert A, et al. Kautschuk Gummi Kunststoffe; 2010. Accepted.
[46] Wilhelm M, Reinheimer P, Ortseifer M. Rheol Acta 1999;38:349–56.
[47] Lebedkin S, Schweiss P, Renker B, Malik S, Hennrich F, Neumaier M, et al. Carbon 2002;40:417–23.
[48] Bahr JL, Mickelson ET, Bronikowski MJ, Smalley RE, Tour JM. Chem Commun 2001;2:193–5.
[49] Rasband WS, Image J. U.S. National institutes of health, http://rsb.info.nih.gov/ij/; 1997–2009. Bethesda, Maryland, USA.
[50] Zhang Q, Fang F, Zhao X, Li Y, Zhu M, Chen D. J Phys Chem B 2008;112:12606–11.
[51] Wood-Adams P, Dealy JM, de Groot AW, Redwine OD. Macromolecules 2000;33:7489–99.
[52] Mu M, Winey KI. J Phys Chem C 2007;111:17923–7.
[53] Palza H, Naue IFC, Wilhelm M. Macrom Rapid Comm 2009;30:1799–804.
[54] Lupton JM, Regester JW. Polym Eng Sci; 1965; October:235–45.
[55] Hatzikiriakos SG, Dealy JM. J Rheol 1992;36:845–84.
[56] Brochard F, de Gennes PG. Langmuir 1992;8:3033–7.
[57] Brochard F, Gay C, de Gennes PG. Macromolecules 1996;29:377–82.
[58] Mu M, Winey KI. J Phys Chem C 2004;37:9048–55.
[59] Den Doelder CFJ, Koopmans RJ, Molenaar J, Van de Ven AAF. J Non-New Mech 1998;75:25–41.
[60] Shore JD, Ronis D, Piche L, Grant M. Phys Rev Lett 1996;77:655–8.
[61] Moleenar J, Koopmans RJ, den Doelder CFJ. Phys Rev E 1998;58:4683–91.
[62] Gonzalez R, Woods R, Eddins S. Digital image processing using matlab. U.S: Pearson Prentice Hall; 2004.
[63] Wilhelm M. Macromol Math Eng 2002;287:83–105.
[64] Kim YC, Lee SJ, Kim JC, Cho H. Polym J 2005;37:206–13.
[65] Klimke K, Parkinson M, Piel C, Kaminsky W, Spiess HW, Wilhelm M. Macromol Chem Phys 2006;207:382–95.